Diagnostic Wind Field Modeling for Complex Terrain: Model Development and Testing

D. G. ROSS AND I. N. SMITH

Centre for Applied Mathematical Modelling, Chisholm Institute of Technology, Caulfield East, Vic. 3145, Australia

P. C. MANINS

Latrobe Valley Airshed Study, Environment Protection Authority, Olderfleet Buildings, Melbourne, Vic. 3000, Australia

D. G. FOX

Rocky Mountain Forest and Range Experiment Station, U.S. Forest Service, Fort Collins, Colorado 80526

(Manuscript received 26 December 1986, in final form 17 June 1987)

ABSTRACT

A three dimensional diagnostic wind field model is shown to be capable of generating potential flow solutions associated with simple terrain features. This is achieved by modifying an initially uniform background wind to make the flow divergence free. Atmospheric stability effects can be incorporated by considering the relative degree of adjustment that is allowed between the horizontal and vertical components of the wind.

A framework for developing a Froude-number-dependent expression for this ratio is proposed and evaluated by comparing modeled streamline deflections of flow past an ideal hill with results from wind tunnel and tow tank experiments.

1. Introduction

Knowledge of the full three-dimensional wind field is important if predictions of air pollutant transport are to be made. This knowledge is invariably limited due to sparse observations, particularly in regions of complex terrain. Predictive models are, in general, time consuming and impractical for real-time applications. Diagnostic wind models however, can quickly and efficiently utilize available observational data to generate a wind field which satisfies some physical or dynamic constraint(s). Kitada et al. (1983) has identified four classifications of diagnostic models, all of which use the continuity equation as the constraint equation in order to ensure that the final wind field is divergence free; however all of these differ in the manner in which this is achieved.

An existing model, ATMOS1, developed by Davis et al. (1984) has been used in the present study as a framework within which to investigate alternative calculation components and to develop and validate an improved model called NUATMOS. The model ATMOS1 was chosen largely because it employs terrain-following coordinates and variable vertical grid spacing, features that are essential to adequately incorporate complex terrain.

Corresponding author address: Dr. D. G. Ross, Centre for Applied Mathematical Modelling, Chisholm Institute of Technology, Caulfield East, Victoria 3145, Australia.

ATMOS1 belongs to Kitada's "Variational Calculus Method" category, the members of which are based on the original concepts of Sasaki (1958, 1970) and their application by Sherman (1978) in developing the operational MATHEW model. Other models which have developed from this approach include a finite element version of MATHEW (Tuerpe and Gresho 1978) and models developed by Ludwig and Byrd (1980) and Bhumralker et al. (1980) which aim to minimize computational costs. The latter models utilize the linear characteristics of the model by combining solutions from the eigenvectors of the covariance matrix of the input wind component data. The models were demonstrated to be practical and economic for the applications considered but they do not appear to be suitable for dealing with large datasets, especially when vertical profiles are available. In these cases there will be a large number of eigenvectors to consider and the method is unlikely to be more efficient than the more conventional techniques being employed here.

Moussiopoulos and Flassak (1986) present and test two numerical algorithms for the calculation of mass-consistent flow fields using a terrain-following coordinate system. The algorithms are demonstrated to be computationally very efficient for full vectorization on vector computers. Their analysis does not allow control of the relative adjustment of the vertical wind component compared to the horizontal component.

NUATMOS differs from ATMOS1 in a number of respects. The major differences include (a) the adoption

of correct 'terrain-following' boundary conditions for an arbitrary terrain surface; and (b) the development of an objective basis for determining the parameter controlling the adjustment made to the vertical wind component compared to the horizontal component during the divergence reduction phase.

In this paper we describe both the testing of the model against exact solutions for flow past simple topography, and attempts to develop and test an objective basis for including atmospheric stability effects. We begin by describing the formulation of NUATMOS and the basis for simulating potential flow. The model is then tested using a range of three-dimensional terrain shapes. Various approaches to including atmospheric stability effects are considered, with a framework developed and subsequent testing given for one approach for the case of simple flow conditions and topography.

2. NUATMOS

NUATMOS produces a three dimensional mass-consistent wind field based on observations which are arbitrarily located. This is achieved by interpolating throughout the domain of interest, and then making minimal adjustments to eliminate divergence.

The interpolation process will not be discussed since the results described in this paper refer specifically to ideal simple situations where the initial wind field is assumed uniform.

The divergence elimination phase is based on the minimization procedure suggested by Sasaki (1958, 1970) and applied by Sherman (1978) in developing the MATHEW model. The variational problem is to minimize the difference between the initial (interpolated) wind field and the final wind field subject to the constraint that the divergence should vanish.

Mathematically, the problem is to minimize the functional

$$E(u, v, w) = \iiint \{\alpha_1^2(u - u_0)^2 + \alpha_1^2(v - v_0)^2 + \alpha_2^2(w - w_0)^2\}dV$$

subject to the constraint

$$H(u_x, v_y, w_z) = \frac{\partial u}{\partial x} + \frac{\partial v}{\partial y} + \frac{\partial w}{\partial z} = 0,$$

where x and y are the horizontal coordinates, z the vertical coordinate, $\mathbf{V}_0 = (u_0, v_0, w_0)$ the corresponding initial (interpolated) velocity, $\mathbf{V} = (u, v, w)$ the final velocity, and α_1 and α_2 are Gauss precision moduli. We distinguish between the adjustments made to the horizontal and vertical velocity components via different values for α_1 and α_2. Large values imply minimal adjustments (e.g., if the velocity component is known exactly) while small values imply that large adjustments are permitted as a consequence of known observational errors.

Using Lagrange multiplier theory, the constraint equation can be incorporated into the minimization integral by the calculus of variations. The problem becomes one of minimizing the modified functional

$$F(u, v, w, \lambda) = E(u, v, w) + \lambda \iiint H(u_x, v_y, w_z)dV$$
$$= \iiint \left[\alpha_1^2(u - u_0)^2 + \alpha_1^2(v - v_0)^2 + \alpha_2^2(w - w_0)^2 + \lambda\left(\frac{\partial u}{\partial x} + \frac{\partial v}{\partial y} + \frac{\partial w}{\partial z}\right)\right]dV \quad (1)$$

where $\lambda(x, y, z)$ is a Lagrange multiplier.

The Euler-Lagrange equations to be solved are

$$2\alpha_1^2(u - u_0) = \partial\lambda/\partial x, \quad (2a)$$

$$2\alpha_1^2(v - v_0) = \partial\lambda/\partial y, \quad (2b)$$

$$2\alpha_2^2(w - w_0) = \partial\lambda/\partial z \quad (2c)$$

and

$$\partial u/\partial x + \partial v/\partial y + \partial w/\partial z = 0 \quad (3)$$

subject to

$$\lambda(u - u_0) = \lambda\delta u = 0, \quad \lambda(v - v_0) = \lambda\delta v = 0,$$
$$\text{and} \quad \lambda(w - w_0) = \lambda\delta w = 0,$$

on the x, y and z boundaries respectively. This corresponds to either setting $\lambda = 0$ (a "free flow" condition) or requiring that the normal component of the flow at the boundary remains unchanged following the adjustment. Assuming that α_1 and α_2 are constant throughout the domain, Eqs. (2) and (3) can be manipulated to give

$$\frac{\partial^2\lambda}{\partial x^2} + \frac{\partial^2\lambda}{\partial y^2} + \left(\frac{\alpha_1}{\alpha_2}\right)^2\frac{\partial^2\lambda}{\partial z^2} = -2\alpha_1^2\nabla\cdot\mathbf{V}_0. \quad (4a)$$

Without loss of generality, we can let $\alpha = \alpha_1/\alpha_2$ and $\alpha_1 = 1$ so that α represents the relative amount of adjustment of the vertical component to the horizontal component. Equation (4a) can be restated as

$$\frac{\partial^2\lambda}{\partial x^2} + \frac{\partial^2\lambda}{\partial y^2} + \alpha^2\frac{\partial^2\lambda}{\partial z^2} = -2\nabla\cdot\mathbf{V}_0. \quad (4b)$$

This equation can be solved by setting $\lambda = 0$ at the free boundaries and ensuring that $\delta w = \partial\lambda/\partial z = 0$ at the surface. The first condition allows adjustments to be made to the normal component of the velocity at 'flow-through' boundaries, while the latter conditions ensure that the initial vertical velocity is preserved at the terrain surface ($z = z_s$). With MATHEW, the w_0 is initially set to zero and does not necessarily correspond to the "no flow-through" condition required at the surface. This is circumvented by prescribing the terrain surface as a series of "steps" such that $\partial z_s/\partial x = \partial z_s/\partial y = 0$. However, Lewellen et al. (1982) showed that this surface representation leads to large velocity errors near the surface. These problems do not arise with the use of terrain-following coordinates.

As with ATMOS1 we make the following coordinate transformation

$$\tilde{x} = x, \tag{5a}$$

$$\tilde{y} = y, \tag{5b}$$

$$\sigma = (z_t - z)/(z_t - z_s) = (z_t - z)/\pi \tag{5c}$$

where z_t represents the top of the solution domain.

It can be shown that the terrain-following velocity components are

$$\tilde{u} = u, \tag{6a}$$

$$\tilde{v} = v, \tag{6b}$$

$$\tilde{w} = \frac{-1}{\pi}\left(w + \sigma u \frac{\partial \pi}{\partial x} + \sigma v \frac{\partial \pi}{\partial y}\right) \tag{6c}$$

and that by substituting for the various terms in (1), λ is then given by

$$\left(\frac{\partial}{\partial x} - \frac{\sigma}{\pi}\frac{\partial \pi}{\partial x}\frac{\partial}{\partial \sigma}\right)\left(\frac{\partial \lambda}{\partial x} - \frac{\sigma}{\pi}\frac{\partial \pi}{\partial x}\frac{\partial \lambda}{\partial \sigma}\right) + \left(\frac{\partial}{\partial y} - \frac{\sigma}{\pi}\frac{\partial \pi}{\partial y}\frac{\partial}{\partial \sigma}\right) \times \left(\frac{\partial \lambda}{\partial y} - \frac{\sigma}{\pi}\frac{\partial \pi}{\partial y}\frac{\partial \lambda}{\partial \sigma}\right) + \left(\frac{\alpha}{\pi}\right)^2 \frac{\partial^2 \lambda}{\partial \sigma^2} = \frac{-2}{\pi}\left(\frac{\partial \pi \tilde{u}_0}{\partial x} + \frac{\partial \pi \tilde{v}_0}{\partial y} + \frac{\partial \pi \tilde{w}_0}{\partial \sigma}\right) \tag{7}$$

subject to $\lambda(\delta \tilde{u}) = 0$, $\lambda(\delta \tilde{v}) = 0$ and, $\lambda(\delta \tilde{w}) = 0$ on the x, y and σ boundaries, respectively. The essential difference between NUATMOS (or ATMOS1) and MATHEW is that with terrain-following coordinates we can prescribe $\tilde{w}_0 = 0$ and $\delta \tilde{w} = 0$ at $\sigma = 1$, which are the free-slip conditions for an arbitrary solid surface.

Moussiopoulos and Flassak (1986) adopt a similar approach but do not distinguish between the relative adjustments to the horizontal and vertical velocities. Kitada et al. (1983) and Kitada et al. (1986) also use terrain-following coordinates but minimize with respect to $\tilde{u}$, $\tilde{v}$ and $\tilde{w}$ rather than the Cartesian velocities. This approach effectively leads to a set of equations and boundary conditions similar to those solved by the MATHEW code but does not readily lead to the potential flow solutions which form the basis of the tests reported here. In addition, α takes on a slightly different interpretation and they propose that a typical value corresponds to the ratio to be expected between vertical and horizontal velocities in the atmosphere (i.e., $\sim$0.01). For the simple flow cases reported here it will be shown that α is more likely to have values between 0.1 and 1.

3. Testing—potential flow solutions

Since diagnostic wind field models (such as NUATMOS) are intended to be used in a routine capacity, it is important that they can be validated in some fashion. This is not always possible other than by cursory means and it may be possible that the results appear plausible despite the existence of subtle logic or coding errors. Here we show theoretically that the minimization process can yield potential flow solutions for simple topographic shapes and that the model does indeed provide satisfactory numerical solutions.

Lewellen et al. (1982), in investigating the Cartesian code MATHEW pointed out that for $\alpha = \alpha_1 = \alpha_2 = 1$,

$$\nabla^2 \lambda = -2 \nabla \cdot \mathbf{V}_0, \tag{8}$$

and that if $\nabla \cdot \mathbf{V}_0 = 0$, then λ represents a velocity potential. Thus, if $\mathbf{V}_0$ represents a uniform background wind, the resulting solution to the problem, subject to no normal flow through the terrain boundary, will be the potential flow field. Testing revealed that the representation of the surface by a series of rectangular blocks always led to errors of O(1) near the surface.

In general, if the initial wind satisfies

$$\mathbf{V}_0 = (u_0, v_0, w_0): u_0 = u_0(x), \quad v_0 = v_0(y) \quad \text{and} \quad w_0 = w_0(z) \tag{9}$$

then the final wind satisfies

$$u = \frac{\partial \phi}{\partial x}, \tag{10a}$$

$$v = \frac{\partial \phi}{\partial y}, \tag{10b}$$

$$w = \frac{\partial \phi}{\partial z} \tag{10c}$$

where

$$\phi = \int u_0 dx + \int v_0 dy + \int w_0 dz + \frac{\lambda}{2}.$$

It also follows that

$$\nabla^2 \phi = \nabla \cdot \mathbf{V}_0 + \tfrac{1}{2} \nabla^2 \lambda = 0 \tag{11}$$

and, therefore, the resultant wind field corresponding to (10) will represent potential flow. If we intend to simulate potential flow, the initial wind field in terrain-following coordinates is prescribed as follows:

$$\left.\begin{aligned} &\bar{\mathbf{V}}_0 = (\tilde{u}_0, \tilde{v}_0, \tilde{w}_0): \tilde{u}_0 = u_0, \quad \tilde{v}_0 = 0 \\ &\text{and} \\ &\tilde{w}_0 = -\sigma \frac{u_0}{\pi}\frac{\partial \pi}{\partial x} \quad (\text{i.e., } w_0 = 0 \text{ for } \sigma < 1) \end{aligned}\right\}. \tag{12}$$

The presence of any terrain surface will induce convergence/divergence which must be eliminated. Thus $\tilde{u}_0$, $\tilde{v}_0$ and $\tilde{w}_0$ will be adjusted within the domain, and at the surface ($\sigma = 1$) where $\tilde{w}_0 = 0$, we require $\delta \tilde{w} = 0$, which leads to the following lower boundary condition:

$$\frac{\partial \lambda}{\partial \sigma} = \frac{\pi[(\partial \pi/\partial x)(\partial \lambda/\partial x) + (\partial \pi/\partial y)(\partial \lambda/\partial y)]}{\alpha^2 + (\partial \pi/\partial x)^2 + (\partial \pi/\partial y)^2}.$$

The adjustments to the initial wind field can be interpreted as the imposition of a "terrain effect" upon a uniform background wind. This leads to speed-up, retardation and channeling as the wind encounters changes in the shape of the underlying terrain surface.

Since analytical solutions are available for potential flow around simple objects, these provide an opportunity to test the model. In addition, potential solutions are relevant to flow past obstacles in neutral conditions and therefore NUATMOS should be capable of simulating those situations when only background wind information is available. Furthermore, as will be shown in section 4, the ratio α enables simulations to be made of both neutral and stable flows past an obstacle, which can be compared with field and laboratory observations.

Testing has shown that NUATMOS produces satisfactory results for several simple cases. The first concerns potential flow past a hemisphere while the second concerns flow past a half cylinder. The final test covers a much wider range of three-dimensional hill slopes described by a half ellipsoid with various aspect ratios, but is limited to predicting "speed-up" over the hill shape.

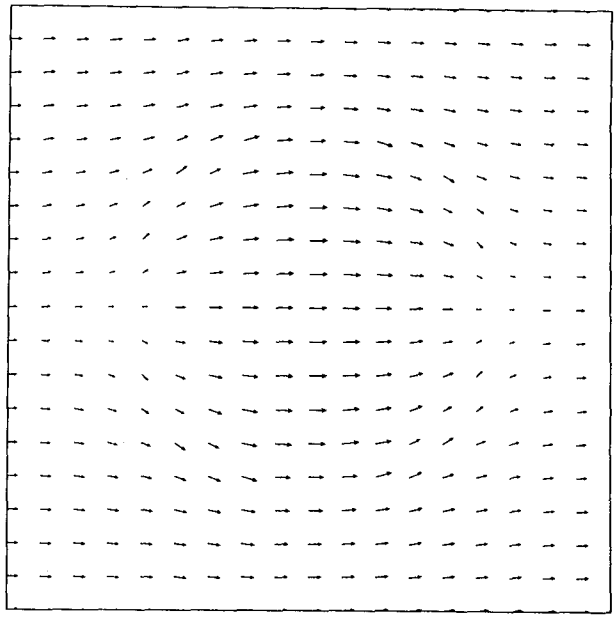

FIG. 1. Near surface velocity vectors for a hemisphere calculated using NUATMOS ($\tilde{w}_0 = -(\sigma u_0/\pi)\partial\pi/\partial x$, Δx = 50 m, background wind speed = 1 m s^{-1}).

a. *Hemisphere tests*

The first simple topographic case study involves a hemisphere of radius 500 m resting on a flat surface with a prescribed background wind of 1 m s^{-1}. The potential flow solution has been simulated with the model using a 37 × 37 horizontal grid with a resolution of 50 m and a logarithmic selection of sigma levels sufficient to provide a close representation near the surface. Figure 1 illustrates the resultant velocity vector field near the surface while Fig. 2 compares the modeled and analytic wind speed values along three (vertical, longitudinal, and transverse) axes. The vertical profile of wind speed above the summit is well reproduced with a surface maximum of 1.53 m s^{-1} representing an overestimate of 0.03 m s^{-1} or only 2%. Similarly, the longitudinal and transverse profiles of the wind speed are also well reproduced, particularly in the vicinity of the "stagnation" points at the perimeter of the hemisphere.

b. *Half-cylinder*

The second case study involves an infinitely long half-cylinder of radius 500 m resting on a flat plain with a prescribed wind of 1 m s^{-1} perpendicular to the axis. A similar grid is again used with a horizontal grid resolution of 50 m. Figure 3 shows the resultant velocity vector fields near the surface and indicates that at the intersection of the lateral boundaries and the cylinder, the adjustment process results in nonzero v components. This occurs because adjustments are permitted at the 'flow-through' boundaries. Along a central longitudinal axis, sufficiently distant from these lateral boundaries, we can reasonably expect the solution to approach the potential flow solution. Figure 4 demonstrates that a good simulation of potential flow is achieved, with stagnation points and speed-up at the summit well represented.

c. *Ellipsoid tests*

In the preceding sections we tested the ability of NUATMOS to simulate the potential flow solution for both a hemisphere and a half-cylinder, where in both cases the complete analytic solution was available. We now describe a further test which covers a much wider range of three-dimensional hill shapes. The potential flow solution is again used as the basis for comparison but, as the complete solution is not readily available, the test is limited to predicting "speed-up" over the hill.

Following Hunt et al. (1978) we consider potential flow over the ellipsoid

$$\frac{x^2}{\ell^2} + \frac{y^2}{b^2} + \frac{z^2}{h^2} = 1 \qquad (13)$$

where ℓ, b, h are the half-widths in the x, y, z directions respectively.

Milne-Thompson (1960, p. 518) shows that the surface velocity is the same at all points on the central plane of the ellipsoid (x = 0), is a maximum, and is given by

$$u = U_{MAX} = 2U_\infty/(2 - \beta_0), \quad v = w = 0, \qquad (14)$$

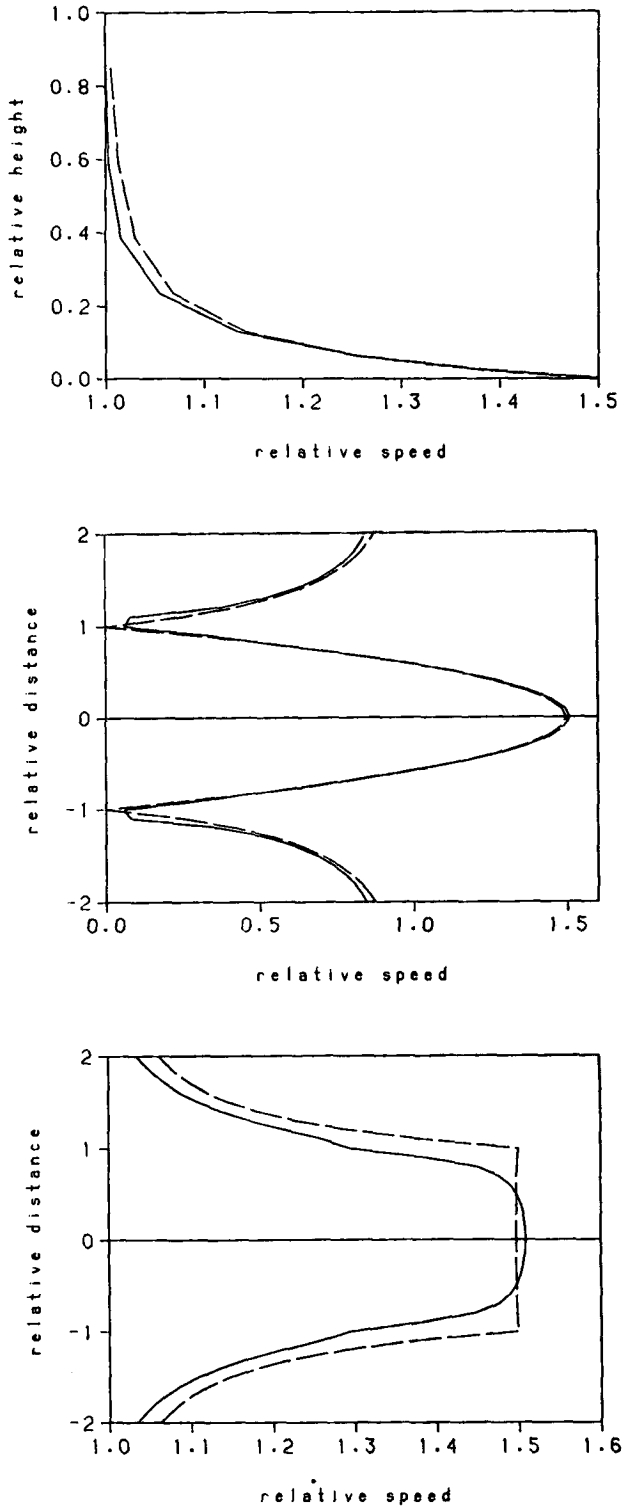

FIG. 2. Wind field for a hemisphere (radius 500 m) as predicted by NUATMOS: Δx = 50 m (solid curve), and the potential flow solution as given by the dashed curve: (a) vertical profile of horizontal wind speed above the summit (total height = 2500 m); (b) wind speed profile along the long-wind horizontal axis (total distance = 4 radii); (c) wind speed profile along the crosswind axis (total distance = 4 radii).

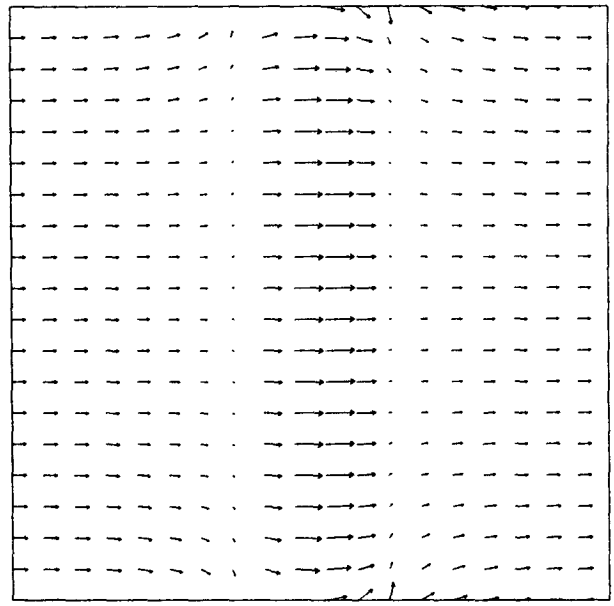

FIG. 3. Near-surface velocity vectors for a half-cylinder (Δx = 50 m and background wind speed = 1 m s^{-1}).

where

$$\beta_0 = \left(\frac{\ell}{h}\right)\left(\frac{b}{h}\right) \times \int_0^\infty \frac{du'}{((\ell/h)^2 + u')^{3/2}((b/h)^2 + u')^{1/2}(1 + u')^{1/2}}, \quad (15)$$

and the upwind flow U_∞ is uniform with height.

Hunt et al., (1978) used this result to determine the "speed-up" defined as

$$S = U_{MAX}/U_\infty \quad (16)$$

for a wide range of ellipsoid dimensions, characterized by the aspect ratios $\xi = b/\ell$ and $\zeta = b/h$.

Figure 5 compares the speed-up predicted by NUATMOS with that determined by Hunt et al., (1978) from (14)–(16) for a wide range of ellipsoid aspect ratios. A similar grid is again used, but with a horizontal grid resolution of 100 m. In each case, there is acceptable agreement between the two (to less than 10%), which provides further evidence of the ability of NUATMOS to simulate potential flow for a wide range of three-dimensional shapes.

Figures 6 and 7 illustrate the flow field produced by NUATMOS for aspect ratio values typical of winds perpendicular and parallel to the longest side of the ellipsoid, respectively. Figure 6, with ξ = 3, produces a speed-up, S = 1.75, which is half-way between that of a sphere and a cylinder. Figures 6a, b illustrate the calculated results at the end of the divergence elimination phase, as well as the initially prescribed wind speed, for the vertical profile of horizontal velocity at the summit of the ellipsoid and the axial flow along

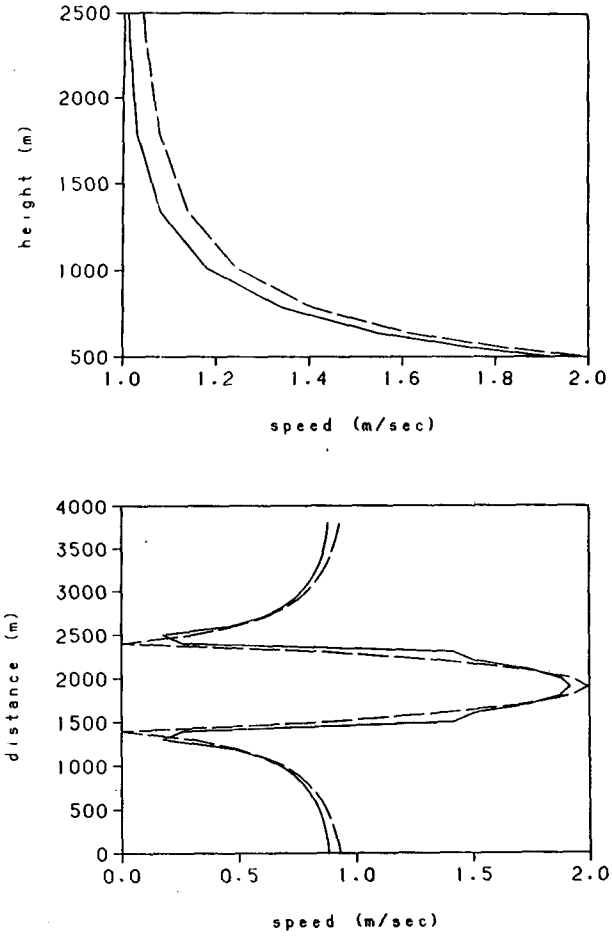

FIG. 4. Wind field for a half-cylinder as predicted by NUATMOS: $\Delta x = 50$ m (solid curve), and the potential flow solution as given by dashed curve: (a) vertical profile of horizontal wind speed above the central summit; (b) wind speed profile along the central longitudinal axis.

the longitudinal axis of the ellipsoid, respectively. Figure 7, with $\xi = 0.25$ and $S = 1.06$, illustrates the reduction of the speed-up as $\xi \to 0$. This behavior is typical of a wind parallel to the longer dimension of the hill, or of separating flow over an approximately symmetrical hill where the effective length of the hill in the direction of the wind is increased.

4. Incorporating atmospheric stablity effects

Two general approaches can be considered for incorporating atmospheric stability effects into NUATMOS. One approach is to extend the formulation to include other relevant physical and dynamic solution constraints such as momentum and energy conservation, the other is to utilize and formalize the role of the parameter α in determining the final velocity field. The value of α governs the amount of adjustment made in the vertical wind component relative to the horizontal adjustment during the divergence-free solution phase. In the limit, as $\alpha \to 0$, the flow becomes essentially two-dimensional at each height (assuming no initial vertical velocities), which is consistent with the first-order flow solution in the limit of low Froude number, i.e., strong stratification (Drazin 1961). Thus, physically, α should be determined by the Froude number characterizing a vertical displacement and the atmospheric stability. It should be noted, however, that α may need to vary across the domain for complex topography since the displacement is different for each terrain feature. Atmospheric stability also varies with height.

The role of α has received little attention in the literature and in most models it has been taken as a constant for the entire domain, (e.g., Sherman 1978; and

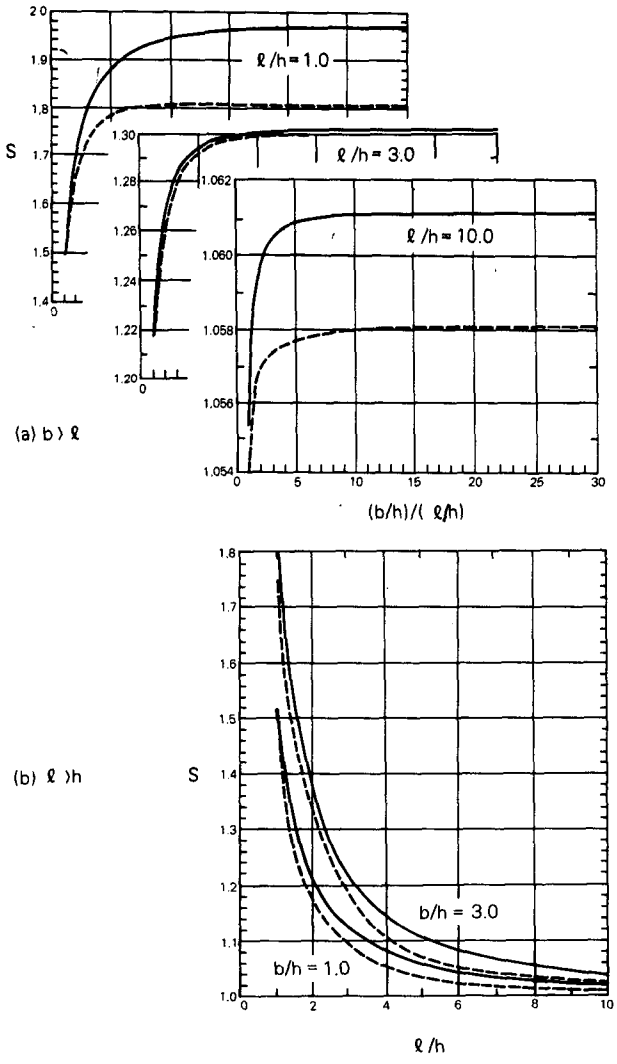

FIG. 5. "Speed up" for potential flow over an ellipsoid hill: calculations of Hunt et al. (1978) (solid curves) and prediction of NUATMOS (dashed curves). (a) $b \geq \ell$, (b) $\ell \geq h$. (N.B., false origins and different scales).

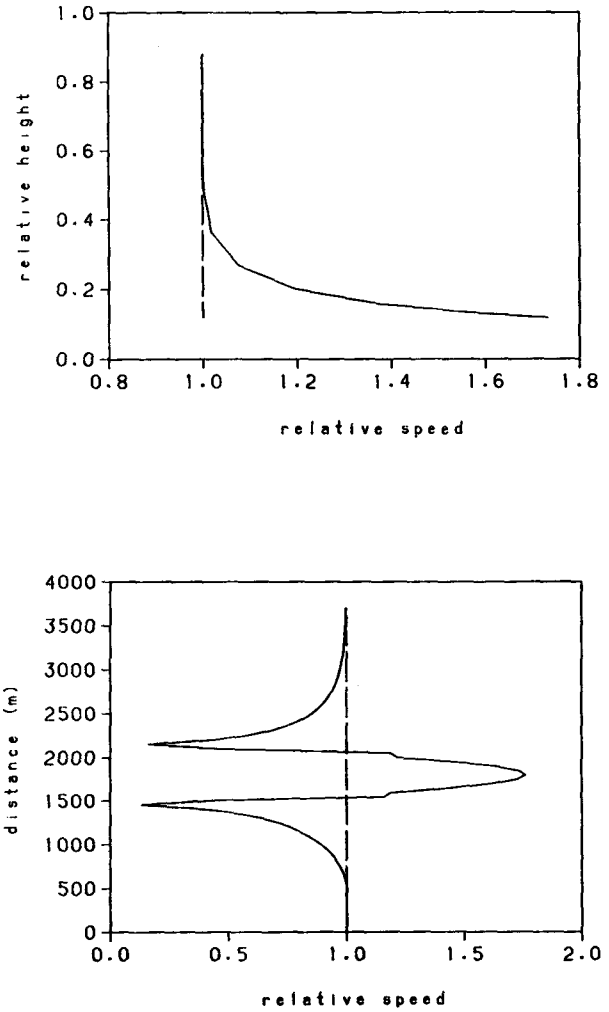

FIG. 6. Predictions of NUATMOS for an ellipsoid with $\xi = 3$ and $\zeta = 3$ ($h = 300$, $b = 900$, $\ell = 300$). The solid line represents the divergence free solution predicted by NUATMOS. The dashed line is the initial velocity: (a) vertical profile of horizontal wind speed above the summit (total height = 2500 m); (b) "speed up" of horizontal velocity along the longitudinal axis of the ellipsoid.

Davis et al. 1984) with a value which is determined subjectively. In these cases the value for α has been chosen to reflect the accuracy of the initial interpolated wind field and is not strictly an indication of stability.

In this section we develop an argument relating α and a Froude number characterizing the domain of interest. The discussion parallels the argument of Snyder et al. (1985) but is slightly more general. The relation is established using experimental results from Hunt and Snyder (1980) for a uniform background flow over a three-dimensional axisymmetric polynomial hill.

Following Sheppard (1956) we can write the equation of mechanical energy for a parcel of air of unit mass in a frictionless gravitational atmosphere as

$$-\frac{dp}{\rho} = d\left(\frac{1}{2}q^2 + gz\right) \tag{17}$$

where $-dp/\rho$ (p is the pressure, ρ the density) is the work done on the parcel by the pressure drop along an increment of path, and the right-hand side of (17) is the change in the kinetic energy ($q^2 = (u^2 + v^2 + w^2)$) plus the potential energy (g is gravity and z height).

We assume that the environment is in a hydrostatic state described by

$$-dp_e = g\rho_e dz \tag{18}$$

where the subscript e is used to denote an environmental property and the parcel moves such that the pressure on the parcel at any level is the pressure at the same level in the environment. Then we can combine (17) and (18) to obtain

$$d\left(\frac{1}{2}q^2\right) = g\frac{\rho_e - \rho}{\rho}dz = g\frac{\theta - \theta_e}{\theta_e}dz, \tag{19}$$

where we have used the gas law and Poisson's equation for potential temperature, θ.

If we further assume the motion of the parcel to be adiabatic (θ constant) and that during a vertical displacement $\eta = z - H_s$ of the parcel from its initial level $z = H_s$, the environmental potential temperature is $\theta_e(z) = \theta + (z - H_s)d\theta_e/dz$, then (19) becomes

$$d\left(\frac{1}{2}q^2\right) = -g\frac{(z - H_s)}{\theta_e}\frac{d\theta_e}{dz}dz. \tag{20}$$

Integration of (20) yields

$$\frac{1}{2}q^2 + g\int \frac{z - H_s}{\theta_e}\frac{d\theta_e}{dz}dz = B, \tag{21}$$

where B is a constant, called the Bernoulli constant,

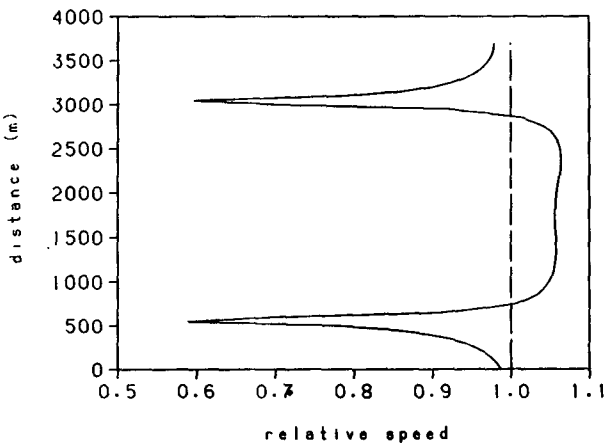

FIG. 7. Predictions of NUATMOS for an ellipsoid with $\xi = 0.25$ and $\zeta = 1$, ($h = 300$, $b = 300$, $\ell = 1200$). "Speed-up" of horizontal velocity along the longitudinal axis of the ellipsoid. The solid line represents the divergence free solution predicted by NUATMOS. The dashed line is the initial velocity.

for the parcel. It is the kinetic energy of the parcel before vertical displacement, i.e., at level $z = H_s$, and the limits of integration are from this level to $z = H_s + \eta$.

Consider the case of wind, with a far upstream velocity field $(u_\infty(z), v_\infty(z), 0)$, and temperature $\theta(z) = \theta_e(z)$ which approaches some arbitrary terrain shape as sketched in Fig. 8. A streamline beginning far upstream at reference level $z = H_s$ will have a value B (from (21)) of

$$B = \frac{1}{2} q_\infty{}^2 = \frac{1}{2}(u_\infty{}^2 + v_\infty{}^2) \approx \frac{1}{2} q^2 + g \int \frac{(z - H_s)}{\theta_e} \frac{d\theta_e}{dz} dz.$$

Thus the change in B at any point along this streamline, due to the change in flow field to account for the effects of terrain and thermal stability, can be written as

$$\Delta B \approx \frac{1}{2}(u^2 - u_\infty{}^2) + \frac{1}{2}(v^2 - v_\infty{}^2) + \frac{1}{2} w^2 + g \int \frac{(z - H_s)}{\theta_e} \frac{d\theta_e}{dz} dz. \quad (22)$$

In principle, conservation of mechanical energy would require $\Delta B = 0$. However, the presence of terrain induces pressure perturbations which are reflected in the thermal stratification [via Eq. (18)] and these extend far upstream. In the presence of stratification, these perturbations can only be found by a complete solution to the problem. For potential flow the pressure perturbations have been shown to lead to speed-up over the terrain (see section 3).

Equation (22) can also be interpreted as the change required from a first-guess field $(u_0, v_0, w_0(x, y, z)) = (u_\infty(z), v_\infty(z), 0)$ for the wind at any point. Then ΔB will be nonzero due to this inexactness, and for the reason mentioned above.

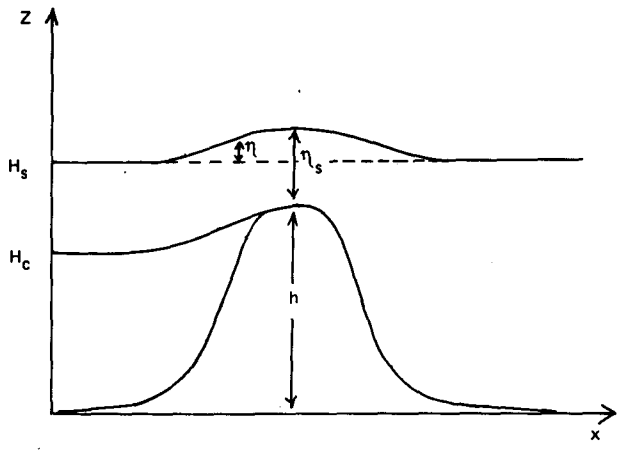

FIG. 8. Coordinates and notation for flow over a polynomial hill.

We define

$$D = \frac{(u_\infty{}^2 - u^2) + (v_\infty{}^2 - v^2)}{2g \int ((z - H_s)/\theta_e)(d\theta_e/dz) dz} \quad (23)$$

where D represents the change in the square of the local Froude number at level z due to a vertical displacement $\eta = z - H_s$ from its upstream value to its value in the vicinity of the terrain feature. We can write, using (23) and (22),

$$\frac{2\Delta B}{1 - D^{-1}} = (u^2 - u_\infty{}^2) + (v^2 - v_\infty{}^2) + \frac{w^2}{1 - D^{-1}} \quad (24)$$

and use the function in (24) as the minimization kernel for our wind determination procedure, subject to the constraint that the divergence should vanish. This approach minimizes the change in kinetic energy due to vertical displacement as a result of the presence of the terrain in a stable environment by minimizing the (weighted) velocity changes. We identify (u_0, v_0, w_0) with $(u_\infty, v_\infty, 0)$, as mentioned above.

Using Lagrange multiplier theory the constraint equation can be incorporated into the minimization integral to yield the modified functional (c.f. section 2, Eq. 1):

$$\iiint \left[(u^2 - u_0{}^2) + (v^2 - v_0{}^2) + \frac{w^2}{1 - D^{-1}} + \psi\left(\frac{\partial u}{\partial x} + \frac{\partial v}{\partial y} + \frac{\partial w}{\partial z}\right)\right] dV, \quad (25)$$

where $\psi(x, y, z)$ is the Lagrange multiplier.

The Euler–Lagrange equations resulting from this approach are complex and ought to be solved iteratively since the local departure of the final streamline from its initial reference level depends upon the vertical velocity along the streamline as follows:

$$\eta(s) = z - H_s = \int_{-\infty}^{s} w ds,$$

where s is a horizontal distance along the streamline direction. Instead, we simplify (25) by approximating D by a value characteristic of the domain.

We first observe that the integral formula derived by Snyder et al. (1985) for calculating the height of the dividing streamline in stable flow over hills,

$$q^2(H_c) \geq 2g \int_{H_c}^{h} \frac{(z - H_s)}{\theta_e} \frac{d\theta_e}{dz} dz, \quad (26)$$

follows from (22) if we choose the reference level H_s as the upstream height of the dividing streamline H_c, approaching a stagnation point on the top of a hill height h, as sketched in Fig. 8. The inequality acknowledges that ΔB is nonzero due to upstream influences. Further, for uniform approach-flow speed U_∞, and a linearly thermally stratified environment characterized

by a buoyancy frequency $N^2 = [(g/\theta_R)(d\theta_e/dz)]$, where θ_R is a representative potential temperature of the air between heights $z = H_s$ far upstream and $z = h$, (26) yields the well-known simple form for displacement of the critical streamline, as discussed in Hunt and Snyder (1980):

$$\left.\begin{aligned} &\eta_c \leqslant hF_h, \\ \text{or} \quad &H_c \geqslant h(1 - F_h), \end{aligned}\right\} \tag{27}$$

where $F_h = U_\infty/Nh$ is the hill Froude number based on the typical terrain height, h. Then at heights $z \leqslant H_c$ we have ${u_\infty}^2 - u^2 \sim {U_\infty}^2$, so $D \approx {U_\infty}^2/{\eta_c}^2N^2$ and from (27) $D \to 1$. Though recognizing that speed-up over the terrain can occur, at heights $z > H_c$, we will use the general scale speed U_∞ and vertical displacement scale $\eta \sim h$; then

$$D \sim \frac{{U_\infty}^2}{N^2h^2} = \frac{{F_h}^2}{a}$$

where a is a scale coefficient which is probably a function of F_h, but will, for simplicity, be taken as a constant here. It should be noted that the scaling $\eta \sim h$ will break down in the limit of strong stability since the streamlines then remain essentially horizontal. In summary, we take

$$\left.\begin{aligned} &D \to 1, \quad z \leqslant H_c \\ &D = {F_h}^2/a, \quad z > H_c \end{aligned}\right\}. \tag{28}$$

Then for $z > H_c$, (25) becomes

$$\iiint \left[(u^2 - {u_0}^2) + (v^2 - {v_0}^2) + \frac{w^2}{1 - aF_h{}^{-2}} + \psi\left(\frac{\partial u}{\partial x} + \frac{\partial v}{\partial y} + \frac{\partial w}{\partial z}\right)\right] dV. \tag{29}$$

(The case $z \leqslant H_c$ will be stated later.)

The associated Euler–Lagrange equations whose solution minimizes the simplified form of (29) are (3) and

$$\left.\begin{aligned} 2u &= \frac{\partial \psi}{\partial x}, \\ 2v &= \frac{\partial \psi}{\partial y}, \\ \frac{2w}{1 - aF_h{}^{-2}} &= \frac{\partial \psi}{\partial z} \end{aligned}\right\}. \tag{30}$$

The equation for ψ may be obtained by eliminating u, v and w from (30) and (3):

$$\frac{\partial^2 \psi}{\partial x^2} + \frac{\partial^2 \psi}{\partial y^2} + (1 - aF_h{}^{-2})\frac{\partial^2 \psi}{\partial z^2} = 0, \tag{31}$$

with associated boundary conditions $\psi\delta u = \psi\delta v = \psi\delta w = 0$ on the x, y and z boundaries, respectively.

If we define

$$\psi = \lambda + \int u_0 dx + \int v_0 dy,$$

where λ is the Lagrange multiplier defined by (4b) and associated with the functional defined by (1), then ψ is a solution of (31) and associated boundary conditions if we equate

$$\alpha^2 = \begin{cases} 1 - aF_h{}^{-2}, & z > H_c \\ 0, & z \leqslant H_c. \end{cases} \tag{32}$$

Thus we have a means of calculating α from a knowledge of the bulk or hill Froude number subject to the determination of the scale coefficient a. We can use the experimental results of Hunt and Snyder (1980) for the displacement of streamlines over a simple axisymmetric hill as a function of the hill Froude number to examine the validity of relation (32) and to determine an appropriate value of the coefficient a. The experimental results were obtained from wind tunnel experiments (neutral flow) and experiments in both small and large tow tanks (neutral and stably stratified flows). The shape of the hill used in the experiments approximated the fourth order polynomial $f(r) = h/[1 + (r/h)^4]$, where $r^2 = x^2 + y^2$ and h is the hill height. The hill Froude number was defined as $F_h = U_\infty/hN$ as before.

In the tests, NUATMOS has been used to generate three-dimensional velocity fields over the polynomial hill, described above, based on an initial uniform background wind, for a variety of values of the parameter α (including the potential flow solution with $\alpha = 1$). Figure 8 illustrates the coordinates and notation used. Having calculated the velocity field for a particular value of α, the streamlines in a vertical section $y = 0$ are then used to calculate η_s, the height of a streamline above the summit of the hill, for various initial heights H_s. The procedure is repeated for various α values in the range $0 < \alpha \leqslant 1$.

The results of this procedure are illustrated in Fig. 9, where the "predicted" results have been superimposed on the experimental results of Hunt and Snyder (1980). The asymptote $\eta_s/h = (H_s/h) - 1$ corresponds to a streamline whose initial height is sufficiently high not to be deflected by the terrain.

For the case of potential flow with $\alpha = 1$, the predicted speed-up of 1.33 compares well with that determined experimentally, viz. 1.27. The characteristic Froude number in relation (32) matches the hill Froude number used in the experiments so the results in Fig. 9 allow us to begin to examine the validity of the form of relation (32) and to determine a value for the coefficient a. There is good agreement, with respect to shape and behavior, between the predictions and experiments for the limited range of H_s/h for which experimental results are presented.

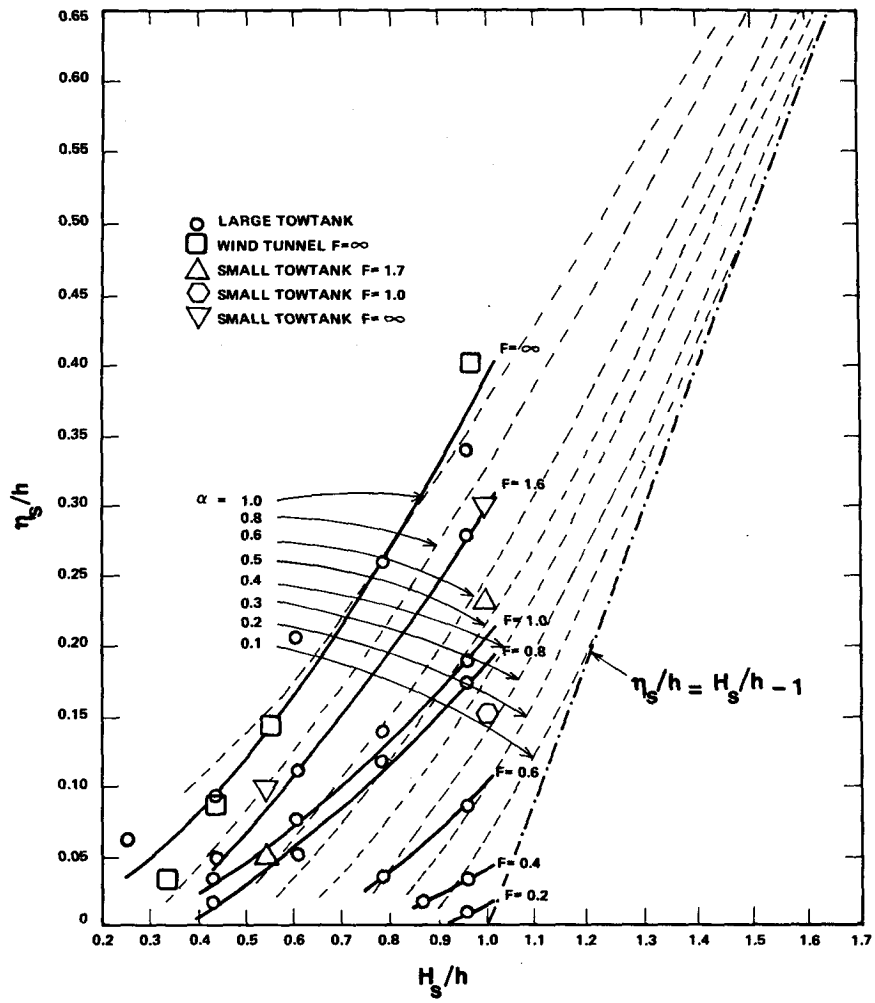

FIG. 9. "Predicted" height of a streamline (η_s) above the hill crest (height = h) for various initial streamline heights (H_s) and values of α (dashed curve), superimposed on the experimental results of Hunt and Snyder (1980) (solid curve).

In Fig. 10 the corresponding values of α^2 and F_h for the data points in Fig. 9 are plotted against each other, excluding values at small H_s/h for which calculation errors are large. Clearly, the scatter is undesirably large, so there is no point in attempting a precise functional description. The functional given in (32) with $a = 0.6$ is shown to be inadequate for data points with $F_h > 1$ (except in the neutral flow limit, $F_h = \infty$), and goes negative for $F_h \approx 0.8$. It is clear that the scale coefficient a varies considerably between experiments and is a strong function of F_h and possibly other factors.

A comparison of alternative functionals to (32) indicates that

$$\alpha^2 = \begin{cases} 1 - a/\sqrt{F_h}, & z > H_c \\ 0, & z \leqslant H_c \end{cases} \tag{33}$$

where a a value of about 0.7 is reasonable but, as expected, is not good at very small values of the hill Froude number. This is because the scaling $\eta \sim h$ breaks down in the limit of strong stability since the streamlines then remain essentially horizontal. This functional with $a = 0.7$ is also shown in Fig. 10. It is adequate for $F_h > 0.4$ but goes negative at lower F_h. This is unrealistic. If more data were available it would be worth investigating further.

We conclude that (33) with $a = 0.7$ provides an adequate description of the relationship between α and atmospheric stability for the simple topography and uniform background flow conditions for which the experiments are valid. The next stage would be to conduct further testing of this approach for the case of real terrain using available field data. Specifically, measurements of vertical velocity would provide a direct comparison with the model "predictions".

A suggested approach to apply this scheme to practical applications is as follows:

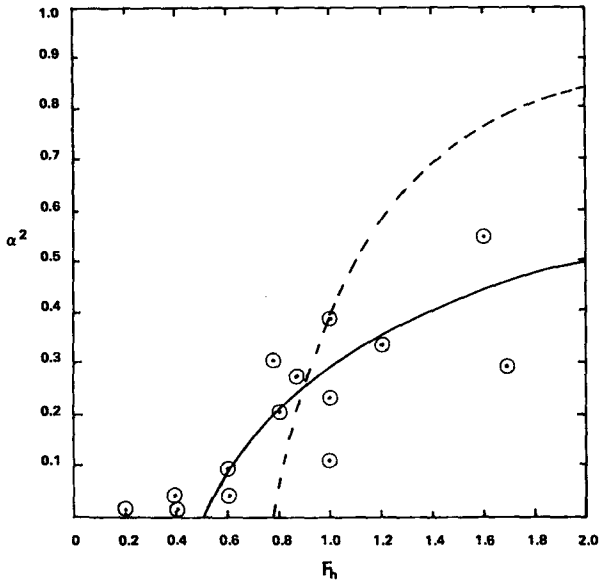

FIG. 10. Comparison of alternative functional relationships between α^2 and F_h with "experimental" data points. Functional (32) with $a = 0.6$ given by dashed curve. Functional (33) with $a = 0.7$ given by solid curve.

1) A vertical sounding of temperature (or otherwise) can be used to divide the air mass in the region into a small number of layers (ℓ_1, ℓ_2, . . .) where ℓ_1 is the thickness of the layer adjacent to the surface, etc., on the basis of the different buoyancy frequencies (N_1, N_2, . . .) characterizing the layers. The terrain may be characterized by a height scale h, the selection of which is generally obvious. Then a unique Froude number for each layer in (33) may be calculated from the initial wind speeds assigned to each layer (U_1, U_2, . . .) as follows:

(a) For all layers i that are below $z = h(1 - F_i)$, $\alpha = 0$ [Equation (32)]. For all remaining layers j that are impinged upon by terrain height h, the length scale for the Froude number is h so

$$F_j = U_j/(N_j h).$$

(b) For all layers k that are fully above the characteristic terrain height then the Froude number is based on the layer thickness, so

$$F_k = U_k/(N_k \ell_k).$$

2) These different Froude numbers are used in (33) to obtain the solution in the usual manner. The new procedure based on a variable Froude number with height is equivalent to choosing different Gauss precision moduli (α_2 compared with α_1) on the basis of the effect of thermal stratification on the relative importance of vertical to horizontal velocities, as given by (33).

An important physical feature for stable flow in complex terrain is the generation of mountain waves in the lee of obstacles. Theoretical and experimental results for the case of simple isolated obstacles of the type referred to in this paper (e.g., Smith 1980; and Rowe et al. 1981) have shown that in contrast to potential flow, the streamline pattern is not symmetric. In particular, streamlines can come very close to the surface on the leeward side of an obstacle. This effect can produce major consequences with respect to the ground level concentration from a plume embedded in such a flow field. Diagnostic models such as NUATMOS can only show this physical feature if it is reflected in the input observations since they do not explictly address momentum conservation.

Fosberg (1984) has attempted to incorporate momentum conservation by combining a diagnostic model with the numerical model for mountain waves developed by Onishi (1969). This model has been used as part of a study to determine potential air pollution impacts of a proposed aluminium smelter in New Zealand (Fosberg and Wratt 1984). Preliminary testing has indicated that the concept of incorporating mountain waves via momentum conservation has great merit but may require further development to be incorporated into a full three-dimensional model.

5. Conclusion

A key component of any air quality model for complex topography is the wind field model used to simulate the advection of pollutants.

In principle, calculating the wind field in complex topography is a solvable problem. Unfortunately, the complexity of the problem is such that it cannot truly be simulated from first principles. Meteorological influences on scales above those resolved by the model and turbulence on scales below those resolved by the model both must be properly parameterized. Even when this is done practical considerations often make numerical solutions of the governing equations impracticable. As a result, simple 'diagnostic' models based on the use of available data in conjunction with interpolation and objective analysis procedures have been developed.

The NUATMOS model has been tested in detail by comparing divergence-free wind solutions against known potential solutions for flow past simple topographic elements. The tests include potential flow past a hemisphere and half-cylinder and a much wider range of three-dimensional hill shapes described by a half-ellipsoid with various aspect ratios. The tests have revealed that the model correctly yields numerical solutions as predicted by theory and that the only limitations are those imposed by resolution and boundary effects. In addition, potential flow solutions, themselves, are relevant to flow past obstacles in neutral conditions, and therefore the tests have demonstrated that NUATMOS is capable of simulating those situations when only background wind information is available.

Conservation of energy arguments have been used to develop a framework for relating the parameter α and a Froude number characterizing atmospheric stability. An initial relationship, and an improved one which satisfies the neutral and strong stability limits, have been proposed within this framework and tested using available laboratory results. The results have identified the range of applicability of the relationships and indicated that an extension to real atmospheric situations is justified. Further developmental work, testing using field data for complex terrain, and incorporation into an operational version of NUATMOS is ongoing.

Acknowledgments. This work was supported by the Department of Resources and Energy under National Energy Research, Development and Demonstration Council Grant 837, and by the U.S. Forest Service under Co-operative Agreement 28-C4-322. We are grateful to Dr. Mark Thompson for his considerable contribution to the initial testing of ATMOS1 and to Dr. Graeme Lorimer for his helpful discussions and assistance with the graphics. We are also grateful for the helpful comments by a referee.

REFERENCES

Bhumralkar, C. M., R. L. Mancuso and F. L. Ludwig, 1980: A practical and economic method for estimating wind characteristics at potential wind energy conservation sites. *Sol. Energy,* **25,** 55–65.

Davis, C. G., S. S. Bunker and J. P. Mutschlecner, 1984: Atmospheric transport models for complex terrain. *J. Climate Appl. Meteor.,* **23,** 235–238.

Drazin, P. G., 1961: On the steady flow of a fluid of variable density past an obstacle. *Tellus,* **13,** 239–251.

Fosberg, M. A., 1984: A diagnostic three-dimensional mass and momentum conserving wind model for complex terrain. *Third Conf. on Mountain Meteorology,* Portland, Amer. Meteor. Soc.

——, and D. S. Wratt, 1984: Modelling wind and transport patterns at Aramoana. *N.Z. J. Sci.,* **27**(4), 337–353.

Hunt, J. C. R., and W. H. Snyder, 1980: Experiments on stably and neutrally stratified flow over a model three-dimensional hill. *J. Fluid Mech.,* **96,** 671–704.

——, —— and R. E. Lawson, 1978: Flow structure and turbulent diffusion around a three-dimensional hill: Fluid modelling study on effects of stratification. Part I: Flow structure. U.S. EPA Env. Monitoring Ser. Rep. EPA-600/4-78-041. Res. Tri. Pk., N.C.

Kitada, T., A. Kaki, H. Ueda and L. K. Peters, 1983: Estimation of vertical air motion form limited horizontal wind data—a numerical experiment. *Atmos. Environ.,* **17,** 2181–2192.

——, K. Igarashi and M. Owada, 1986: Numerical analysis of air pollution in a combined field of land/sea breeze and mountain/valley wind. *J. Climate Appl. Meteor.,* **25,** 767–784.

Lewellen, W. S., R. I. Sykes and D. Oliver, 1982: The evaluation of MATHEW/ADPIC as a real time dispersion model. Prepared for U.S. Nuclear Regulatory Comm. NUREG/CR—2199 ARAP Rep. No. 442.

Ludwig, F. L., and G. Byrd, 1980: An efficient method for deriving mass-consistent flow fields from wind observations in rough terrain. *Atmos. Environ.,* **14,** 585–587.

Milne-Thompson, L. M., 1960: *Theoretical Hydrodynamics,* fourth ed., Macmillan Publ., Co.

Moussiopoulos, N., and Th. Flassak, 1986: Two vectorized algorithms for the effective calculation of mass-consistent flow fields. *J. Climate Appl. Meteor.,* **25,** 847–857.

Onishi, G., 1969: A numerical method for three-dimensional mountain waves. *Japan. J. Meteor. Soc.,* **47,** 352–359.

Rowe, R. D., S. F. Benjamin, K. P. Chung, J. J. Havlena and C. Z. Lee, 1981: Field studies of stable air flow over and around a ridge. *Atmos. Environ.,* **16,** 643–653.

Sasaki, Y., 1958: An objective analysis based on the variational method. *J. Meteor. Soc. Japan,* **36,** 77–78.

——, 1970: Some basic formalisms in numerical variational analysis. *Mon. Wea. Rev.,* **98,** 875–883.

Sheppard, P. A., 1956: Airflow over mountains. *Q. Jour. Roy. Meteor. Soc.,* **82,** 528–529.

Sherman, C. A., 1978: A mass-consistent model for wind fields over complex terrain. *J. Appl. Meteor.,* **17,** 312–319.

Smith, R. B., 1980: Linear theory of stratified hydrostatic flow past an isolated mountain. *Tellus,* **32,** 348–364.

Snyder, W. H., R. S. Thompson, R. E. Eskridge, R. E. Lawson, I. P. Castro, J. T. Lee, J. R. C. Hunt and Y. Ogawa, 1985: The structure of strongly stratified flow over hills: The dividing-streamline concept. *J. Fluid Mech.,* **152,** 249–288.

Tuerpe, D. R., and P. M. Gresho, 1978: Variational wind field adjustment over complex terrain using finite element techniques. *Conf. on Sierra Nevada Meteorology,* S. Lake Tahoe, Amer. Meteor. Soc., 68–70.